

Reply to the Comments of the Referee #2

1
2 **1. Introduction: Haze in China is a very hot topic and raises a bunch of new**
3 **studies recently. The authors may cite more recent papers to strengthen this part.**
4 **Climate change (Cai et al., 2017, Nature Climate), Arctic sea ice loss (Zou et al.,**
5 **2017, Science Advances) and decadal weakening of winds (Yang et al., 2016, JGR)**
6 **suggested causes in climate view. Review article on light-absorbing aerosols**
7 **(Qian 2015) and Asian monsoon-aerosol (Li 2016).**

8 **Cai W., et al. (2017), Weather conditions conducive to Beijing severe haze more**
9 **frequent under climate change, Nat. Clim. Change,**
10 **doi:10.1038/nclimate3249.**

11 **Y. Zou, et al. (2017), Arctic sea ice, Eurasia snow, and extreme winter haze in**
12 **China, Sci. Adv., 3, p. e1602751**

13 **Yang, Y., et al. (2016), Increase in winter haze over eastern China in recent**
14 **decades: Roles of variations in meteorological parameters and**
15 **anthropogenic emissions, J. Geophys. Res. Atmos., 121, 13,050–13,065,**
16 **doi:10.1002/2016JD025136.**

17 **Qian Y, TJ Yasunari, SJ Doherty, MG Flanner, WK Lau, J Ming, H Wang, M**
18 **Wang, SG Warren, and R Zhang. 2015. "Light-absorbing Particles in Snow**
19 **and Ice: Measurement and Modeling of Climatic and Hydrological Impact."**
20 **Advances in Atmospheric Sciences 32(1):64-91.**
21 **doi:10.1007/s00376-014-0010-0.**

22 **Li Z, W Lau, V Ramanathan, GX Wu, Y Ding, M Manoj, J Liu, Y Qian, J Li, T**
23 **Zhou, J Fan, D Rosenfeld, Y Ming, Y Wang, J Huang, B Wang, X Xu, SS**
24 **Lee, M Cribb, F Zhang, X Yang, C Zhao, T Takemura, K Wang, X Xia, Y**
25 **Yin, H Zhang, J Guo, P Zhai, N Sugimoto, S Babu, and G Brasseur. 2016.**
26 **"Aerosol and Monsoon Climate Interactions over Asia." Reviews of**
27 **Geophysics 54(4):866-929. doi:10.1002/2015RG000500.**

28
29 *Reply:* The introduction part has been revised as suggestions.

30 **Projected Changes in Haze Pollution Potential in China: An**
31 **Ensemble of Regional Climate Model Simulations**

32
33 Zhenyu Han¹, Botao Zhou^{1,2}, Ying Xu¹, Jia Wu¹, Ying Shi¹

34 ¹National Climate Center, China Meteorological Administration, Beijing, China

35 ² Collaborative Innovation Center on Forecast and Evaluation of Meteorological
36 Disasters, Nanjing University of Information Science & Technology, Nanjing, China

37
38
39
40 **Corresponding author:** Botao Zhou

41 **Corresponding address:** National Climate Center, China Meteorological
42 Administration, Beijing 100081, China

43 **E-mail:** zhoubt@cma.gov.cn

44 **Abstract.** Based on the dynamic downscaling by the regional climate model RegCM4
45 from three CMIP5 global models under the historical and the RCP4.5 simulations, this
46 article evaluated the performance of the RegCM4 downscaling simulations on the air
47 environment carrying capacity (AEC) and weak ventilation days (WVD) in China,
48 which are applied to measure haze pollution potential. Their changes during the
49 middle and the end of the 21st century were also projected. The evaluations show that
50 the RegCM4 downscaling simulations can generally capture the observed features of
51 the AEC and WVD distributions over the period 1986-2005. The projections indicate
52 that the annual AEC tends to decrease and the annual WVD tends to increase almost
53 over the whole country except central China, concurrent with greater change by the
54 late of the 21st century than by the middle of the 21st century. It suggests that annual
55 haze pollution potential would be enlarged under the RCP4.5 scenario as compared to
56 the present. For seasonal change in the four main economic zones of China, it is
57 projected consistently that there would be a higher probability of haze pollution risk
58 over the Beijing-Tianjin-Hebei (BTH) region and the Yangtze River Delta (YRD)
59 region in winter and over the Pearl River Delta (PRD) zone in spring and summer in
60 the context of the warming scenario. Over Northeast China (NEC), future climate
61 change might reduce the AEC or increase the WVD throughout the whole year, which
62 favors the occurrence of haze pollution and thus the haze pollution risk would be
63 aggravated. Relative contribution of different components related to the AEC change
64 further indicates that changes of the boundary layer depth and the wind speed play the
65 leading roles in the AEC change over the BTH and NEC regions. In addition to those

66 two factors, the precipitation change also exerts important impacts on the AEC

67 change over the YRD and PRD zones.

68 **Keywords** air environment carrying capacity, ventilation day, haze pollution potential,

69 regional climate model, evaluation and projection

70

71 **1 Introduction**

72 Haze, as a phenomenon of severe air pollution, exerts remarkably adverse
73 impacts on society and human health, thereby highly concerned by the public and
74 policy makers. Particularly in recent years, heavy haze events hit China frequently
75 (Wang et al., 2014; Zhang et al., 2014) and caused serious damages in many aspects.
76 For instance, they not only increased traffic accidents and delayed traffic (Wu et al.,
77 2005; 2008), but also aggravated ill health problems including respiratory disease,
78 heart disease, cancer and premature death (Wang and Mauzerall, 2006; Xu et al.,
79 2013). Thus, more and more attentions have been paid to the haze pollution in China.

80 The increasing trend of the haze days in China during recent decades (Ding and
81 Liu, 2014; Song et al., 2014) is documented to be largely attributed to human
82 activities. Due to rapid economic development and urbanization, the pollutants
83 emitted into the atmosphere have been increased, consequently resulting in an
84 intensification of haze pollution in China (Liu and Diamond, 2005; He et al., 2013;
85 Wang et al., 2013b; 2016). Climate change also plays an important role (Jacob and
86 Winner, 2009; Wang et al., 2016; [Cai et al., 2017](#)). Some studies have indicated that
87 the reduction of surface wind speed, surface relative humidity and precipitation in
88 recent decades (Gao, 2008; Guo et al., 2011; Jiang et al., 2013; Song et al., 2014;
89 Ding and Liu, 2014; [Yang et al., 2016](#)) provide unfavourable conditions for the
90 sedimentation and diffusion of air pollutants, and thus increase the occurrence of haze
91 pollution in China. Besides, the Arctic sea ice declining under global warming
92 contributes positively to the increase of haze days in eastern China (Wang et al., 2015;

93 | Wang and Chen, 2016; [Zou et al., 2017](#)). Other influential climate factors for the
94 increase of haze pollution in China, such as the weakening of the East Asian winter
95 monsoon (Li et al. 2015; Yin et al., 2015) and the northward shifting of the East Asian
96 jet (Chen and Wang, 2015), are also highlighted. In summary, the combined effects of
97 increased pollutants and climate change are responsible for the haze pollution in
98 China.

99 IPCC AR5 reported that continued emissions of greenhouse gases will cause
100 further changes in all components of the climate system (IPCC, 2013). From the point
101 view of the CMIP5 projected change in climate conditions, there are both positive and
102 negative contributors for the haze pollution in China. For example, the projected
103 increase in precipitation (Xu and Xu, 2012; Tian et al., 2015; Wu et al., 2015b) is
104 expected to reduce haze pollution, whereas the decrease of the Arctic sea ice extent
105 (IPCC, 2013) and the weakening of the East Asian winter monsoon (Wang et al.,
106 2013a) are inclined to increase haze pollution. So, how the haze pollution in China
107 will change under the future warming scenario is still an open issue.

108 Air environment carrying capacity (AEC), which is a combined metric to
109 measure atmospheric capacity in transporting and diluting pollutants into the
110 atmosphere, provides a direct way to investigate the change of the haze pollution
111 potential. When the AEC is low (high), it is unfavourable (favourable) for the
112 diffusion and cleaning of the pollutants, and thus the haze pollution is (not) prone to
113 occur. So far, the AEC has been applied in the operation of China Meteorological
114 Administration (CMA) to forecast haze pollution potential (Kang et al., 2016). On the

115 other hand, CMIP5 global climate models (GCMs) show some limitations in
116 simulating regional climate due to their relatively coarse resolutions (Giorgi et al.,
117 2009). Regional climate models (RCMs) with higher resolutions are demonstrated to
118 outperform global models on the regional scale (Lee and Hong 2014; Wu et al. 2015a;
119 Gao et al. 2012, ~~2016b~~2017). Thus, this study is aimed to project changes of the haze
120 pollution potential in China from the AEC perspective, based on the downscaling
121 simulations of the regional climate model RegCM4 under the RCP4.5 scenario.

122

123 **2 Model, data and method**

124 **2.1 Data, regional climate model and simulations**

125 The regional climate model RegCM4 used in this study is developed by the ICTP
126 (Giorgi et al., 2012) and applied widely around the world. The model has the
127 horizontal resolution of 25 km and 18 vertical sigma layers with the top at 50 hPa.
128 Based on the study of Gao et al. (2016a, ~~2017b~~), we selected a suite of physical
129 parameterization schemes suitable for the simulation of China climate, including the
130 Emanuel convection scheme (Emanuel, 1991), the radiation package of the CCM3
131 model for atmospheric radiative transfer (Kiehl et al., 1998), the non-local formulation
132 of Holtslag (Holtslag et al., 1990) for planetary boundary layer, the SUBEX
133 parameterization for large-scale precipitation (Pal et al., 2000), and the CLM3.5 for
134 land surface process (Oleson et al., 2008). The land cover data were updated based on
135 the vegetation regionalization maps of China (Han et al., 2015).

136 The domain for the downscaling simulations is the region recommended by
137 CORDEX-East Asia phase II (Giorgi et al., 2009), covering China continent and
138 adjacent regions. The RegCM4 simulations, called EC, HAD, and MPI for short, were
139 driven at 6-hourly intervals by the historical (1979-2005) and RCP4.5 (2006-2099)
140 simulations from three CMIP5 global models i.e., EC-EARTH, HadGEM2-ES, and
141 MPI-ESM-MR, respectively. In CMIP5, ~20 GCMs provide the six-hourly outputs of
142 wind speed, temperature, and humidity for dynamical downscaling. However, to drive
143 RCM modeling, the ratio of the resolution between GCMs and RCMs should not
144 exceed 6-8. So, only those GCMs with the resolution of 1~2 degree or higher can be
145 used to drive RegCM4 simulations. Due to the availability of CMIP5 GCMs and
146 considering large volume of outputs for ~120-yr RegCM4 simulations, we just used
147 these three GCMs for this study. The average of the three simulations with equal
148 weight is taken as the ensemble mean. The historical simulation denotes the past
149 climate, and the RCP4.5 represents the medium-low radiative forcing scenario with
150 the radiative forcing peaking at 4.5 Wm^{-2} by 2100 (Taylor et al., 2012). Readers can
151 visit <http://cmip-pcmdi.llnl.gov/cmip5> for the information about the three CMIP5
152 models and the forcing.

153 To validate the performance of the RegCM4 downscaling simulations, the
154 ERA-Interim reanalysis dataset (Uppala et al., 2008) with the horizontal resolution of
155 $0.75^\circ \times 0.75^\circ$ was employed as observations, including 6-hourly boundary layer height,
156 precipitation, geopotential height and wind speed.

157 2.2 Analysis method

158 The AEC considers the processes of wet deposition and ventilation and is
159 expressed in the form:

$$160 \quad AEC = C_s \cdot (W_r \cdot R \cdot \sqrt{S} + \frac{\sqrt{\pi}}{2} \cdot U_{BL} \cdot H) \quad (1)$$

161 where C_s is the standard concentration of air pollutant (here, the value is $75 \mu \text{g m}^{-3}$,
162 standard concentration for $\text{PM}_{2.5}$ in China), W_r is washout constant (6×10^5), R is
163 precipitation, S is unit area and defined as 2500 km^2 , U_{BL} is mean wind speed
164 averaged within the boundary layer, H is boundary layer height (Xu and Zhu, 1989).
165 High (Low) AEC is disadvantageous (advantageous) for the occurrence of haze
166 pollution, indicating low (high) haze pollution potential. It should be pointed out that
167 the AEC measures atmospheric carrying capacity in transporting and diluting
168 pollutants. It does not reflect real emission characteristics. The C_s is the standard
169 concentration of air pollutant not the real concentration of the pollutant emitted into
170 the air. For different pollutants, different value can be fixed for C_s . Because what we
171 concerned in this study is the haze pollution potential, its value is set as the standard
172 concentration for $\text{PM}_{2.5}$ in China.

173 The term $U_{BL} \cdot H$ is named ventilation coefficient (Krishnan and Kunhikrishnan,
174 2004). Large ventilation coefficient means that a deeper boundary layer can dilute
175 pollutants and strong winds can remove local pollutants, unfavourable for the haze
176 occurrence, and vice versa. If each of the 6-hourly ventilation coefficients within one
177 day is less than $6000 \text{ m}^2 \text{ s}^{-1}$, this day is counted as one weak ventilation day (WVD)
178 (Leung and Gustafson, 2005). Longer WVD indicates more haze pollution incidents.

179 The threshold of $6000 \text{ m}^2 \text{ s}^{-1}$ for the ventilation coefficient was widely used not only
 180 in the U.S. (Hanson and McKee, 1983; Leung and Gustafson, 2005; Trail et al., 2013),
 181 but also in other places such as India (Goyal and Rao, 2007; Manju et al., 2002),
 182 Athens (Kassomenos et al., 1995), and Thailand (Pimonsree, 2008). A sensitivity
 183 analysis shows that that there is little change in the relationship between the WVD
 184 and the haze days if using different thresholds to calculate WVD.

185 According to Eq. (1), the AEC change results from changes in precipitation,
 186 wind speed, and boundary layer depth, which can be simplified as:

$$187 \quad \Delta \text{AEC} = \alpha \cdot \Delta R + \beta \cdot \Delta(U_{BL} \cdot H) \quad (2)$$

188 where $\alpha = C_s \cdot W_r \cdot R$, $\beta = C_s \cdot \frac{\sqrt{\pi}}{2}$, and Δ represents the difference between the future and
 189 present-day climate (RCP4.5 minus reference period).

190 The Eq. (2) could be further decomposed as follows:

$$191 \quad \Delta \text{AEC} = \alpha \cdot \Delta R + \{\beta \cdot \Delta U_{BL} \cdot H_{pd} + \beta \cdot (U_{BL})_{pd} \cdot \Delta H + \beta \cdot \Delta U_{BL} \cdot \Delta H + TR\} \quad (3)$$

192 The subscript “pd” denotes the present-day climate. The first to third terms in the
 193 right-hand side are associated with changes in precipitation, wind speed within the
 194 boundary layer, and boundary layer depth, respectively. The fourth term is a nonlinear
 195 term including the contribution of changes in both wind speed and boundary layer
 196 depth. Since we use 6-hourly data for the AEC calculation while monthly mean data
 197 for the diagnosis of the change, the last term TR (transient term, deviation from
 198 monthly mean) cannot be ignored, which is obtained as a residual.

199 The pattern-amplitude projection (PAP) method (Park et al., 2012) is applied to
200 quantify the relative contributions of individual processes P_i to the AEC change over
201 certain region.

$$202 \quad P_i = \frac{\langle \Delta AEC_i \cdot \Delta AEC \rangle}{\langle \Delta AEC \cdot \Delta AEC \rangle} \quad (4)$$

203 in which $\langle \rangle$ represents area mean, ΔAEC_i represents components in the
204 right-hand side of Eq. (3).

205 As stated above, a low (high) AEC are favourable (unfavourable) for the
206 occurrence of the haze pollution. Longer (Shorter) WVD corresponds to more (less)
207 haze pollution incidents. To verify this conclusion, we calculated the quantized
208 relationship of the haze days with the AEC and the WVD during the period
209 1980-2016 in the observation. The data of the haze days, which are based on daily
210 visibility and relative humidity records from ~2400 observation stations in China, are
211 available from the CMA. The correlation analysis does show significantly negative
212 correlations between the haze days and the AEC, and significantly positive
213 correlations between the haze days and the WVD over eastern China where the haze
214 mainly occurs.

215

216 **3 Performance of the downscaling simulations**

217 The performance of the RegCM4 downscaling simulations on the AEC spatial
218 pattern is firstly evaluated through the comparison with the observation. As shown in
219 Fig. 1a, the observed AEC is in general large in western China, with the maxima
220 located over Tibet. Low AEC is found mainly over central and eastern China,

221 northwestern Xinjiang, and parts of Northeast China. The simulated AEC
222 distributions from the ensemble (Fig. 1b) and its members (Fig. 1c-e) show general
223 resemblance to the observation. The spatial correlation coefficients between the
224 simulation and the observation are all higher than 0.75 (Table 1). On the national
225 average, the root mean square error (RMES) is small for the ensemble mean and each
226 member, which varies between 0.47 and 0.53 (Table 1). Nevertheless, there are also
227 some deficits in the simulations. For example, the AEC is underestimated over the
228 southern Xinjiang and overestimated over parts of North China. Our analysis indicates
229 that the simulation bias in boundary layer depth is the major factor for the simulated
230 AEC bias over most parts of China (figure not shown).

231 We further present the observed and simulated distribution of the seasonal AEC
232 in China during 1986-2005. For the observation, the winter AEC is the lowest among
233 the four seasons in a broad region of China (Fig. 2a). In spring, the AEC increases
234 significantly and the regions with high AEC expand obviously. The central eastern
235 China is dominated by the low capacity (Fig. 2c). Compared with the case in spring,
236 the summer AEC increases over central China while decreases slightly over Tibet and
237 Northeast China (Fig. 2e). The AEC distribution in autumn is similar to that in winter
238 but with larger capacity over the regions except Tibet (Fig. 2g). The seasonal
239 variation of the AEC in the ensemble simulation agrees with that in the observation
240 although there are some discrepancies (Fig. 2b, 2d, 2f and 2h). The spatial correlation
241 coefficient between the simulation and the observation ranges from 0.60 to 0.79 and

242 the RMES is in the range of 0.47 to 0.75 for the national average in four seasons
243 (Table 2).

244 The WVD distribution during 1986-2005 in the observation and the ensemble
245 simulation is displayed in Fig. 3a and Fig.3b, respectively. It is noticed that the
246 simulated pattern and the observed pattern are approximate to each other. Namely, the
247 number of weak ventilation days per year is relatively small over Tibet while
248 relatively large over central and eastern China, Northeast China, southern North
249 China and Xinjiang. The spatial correlation between them is 0.75. However, we also
250 note that the WVD is overestimated by the ensemble simulation.

251 The wet deposition is observed to be large over southern China and the south
252 edge of the Tibetan Plateau while small over northwestern China (Fig. 3c). According
253 to Eq. (1), the wet deposition pattern exactly corresponds to the distribution of
254 precipitation. The observed features can also be captured by the ensemble simulation
255 (Fig. 3d). The spatial correlation coefficient between the simulation and the
256 observation is up to 0.85.

257 In brief, the downscaling simulations of the RegCM4 can reasonably reproduce
258 the observed characteristics of the distribution of the AEC, WVC and wet deposition
259 in China. It provides justification to use them for the future projection.

260

261 **4 Projected changes**

262 Fig. 4 exhibits the ensemble projected changes in AEC, WVC and wet deposition
263 during the middle of the 21st century (2046-2065) and the end of the 21st century

264 (2080-2099) relative to the reference period 1986-2005. The periods 2046-2065 and
265 2080-2099 are commonly used to represent near-term and long-term in the CMIP5
266 projection, respectively (IPCC, 2013). A general decrease in AEC and an overall
267 increase in WVC are projected over almost the whole country except central China in
268 the context of the RCP4.5 scenario. The change in magnitude is larger by the end of
269 the 21st century than by the middle of the 21st century. The maximum decrease in
270 AEC appears at the edge of the Qinghai-Tibet Plateau and the Loess Plateau, with the
271 percentage change being 4% for the middle of the 21st century and 5% for the end of
272 the 21st century. The relatively large decreases are located in Southwest China,
273 northern North China, Northeast China and Inner Mongolia (Fig. 4a and Fig.4b). The
274 increase in WVD is projected to be particularly pronounced in western and northern
275 China (Fig. 4c and Fig. 4d). The three ensemble samples agree well on the sign of the
276 changes, indicative of a good consistency in the projection. In contrast, there would be
277 an increasing tendency for the AEC and a decreasing tendency for the WVD over
278 central China where the climatological capacity is low in the reference period
279 1986-2005. However, the sign of the projected change is inconsistent among the three
280 ensemble samples. Compared with the ensemble projection, the EC and HAD show
281 relatively large discrepancy for the sign of the projected change in AEC and WVD,
282 respectively (Figures not shown).

283 For the change in wet deposition, a general increase is projected across China,
284 also with greater change in 2080-2099 than in 2046-2065 (Fig. 4e and Fig. 4f). In
285 addition, we can find inconsistent signs of the projected change over southern China

286 during 2046-2065 (Fig. 4e) and over some parts of Northeast China during 2080-2099
287 (Fig. 4f). The inconsistent during 2046-2065 (2080-2099) is mainly due to the
288 difference of the HAD (MPI) projection from the other two ensemble members
289 (Figures not shown).

290 Following, we turn to examine the seasonal and annual changes of the AEC and
291 WVD over the four main economic zones of China (Fig. 1f) which suffer severely
292 from the haze pollution at present, i.e., Beijing-Tianjin-Hebei region (BTH),
293 Northeast China (NEC), Yangtze River Delta economic zone (YRD), and Pearl River
294 Delta economic zone (PRD) in more detail.

295 1) Beijing-Tianjin-Hebei region

296 As shown in Fig. 5a, the ensemble projection indicates a decrease of the AEC in
297 all four seasons during the middle of the 21st century. The percentage change relative
298 to 1986-2005 is the lowest in spring and the largest in winter. The changes in summer
299 and autumn are between -2% and -3%. The three ensemble members agree on the sign
300 of the changes in all seasons except spring but with different spread. For the summer
301 season, the spread is the smallest. While in other seasons, it is close to or larger than
302 the ensemble projected change. During the end of the 21st century, the decrease of the
303 AEC is further enhanced, with the largest enhancement occurring in winter. Moreover,
304 the spread in general becomes much larger. For annual change, both the ensemble and
305 its members project that the AEC would reduce during the middle and the end of the
306 21st century with the larger amplitude in the latter period.

307 As for the WVD (Fig. 5b), an increasing tendency is projected by the ensemble
308 for annual and seasonal mean during the middle of the 21st century. The change is the
309 smallest in summer and the largest in winter. The ensemble members show good
310 agreement on the positive change in winter, autumn, and annual mean. During the late
311 of the 21st century, the increase in WVD is further enlarged in winter and autumn
312 while it is reduced in spring and summer. There is no appreciable change for annual
313 mean as compared to that in the middle of the 21st century. Only for the winter season
314 and annual mean, all the individual simulations consistently show the same projection
315 as the ensemble.

316 2) Northeast China

317 The annual and seasonal AEC is projected by the ensemble to decrease during
318 the middle of the 21st century, and the percentage changes are comparable among
319 four seasons and annual mean (Fig. 6a). The ensemble members also project negative
320 tendency consistently except in spring. Compared with the middle of the 21st century,
321 the case for the end of the 21st century is similar but with larger decrease. Besides, all
322 the three ensemble members show good consistence for the projection.

323 The WVD is projected by the ensemble and its members to increase during the
324 middle and the end of the 21st century for annual mean and all four seasons (Fig. 6b).
325 Similarly, the projected change is larger during the end of the 21st century than during
326 the middle of the 21st century, with the largest increase appearing in spring.

327 3) Yangtze River Delta economic zone

328 The ensemble projection indicates that the AEC would decrease for annual mean
329 and all the seasons except autumn (Fig. 7a). The percentage change is the smallest in
330 spring (with the decrease of less than 1%) and the greatest in winter (with the
331 decrease of more than 3%). The counterparts for summer and autumn are about -2%
332 and 1%, respectively. However, large spread exists among the projections of the three
333 ensemble members. Only for winter and annual mean, they project the same sign of
334 the change. At the end of the 21st century in the ensemble projection, the decrease in
335 AEC is enhanced to 6% in winter. Consistent change is projected by the ensemble
336 members. In contrast, the decrease in summer and the increase in autumn are
337 weakened as compared to the middle of the 21st century. A slight increase of the AEC
338 is found in spring. For annual mean AEC, the decrease is somewhat larger by the end
339 of the 21st century than by the middle of the 21st century.

340 The WVD for annual mean, winter and spring is projected by the ensemble to
341 increase, with larger change during the end of the 21st century than during the middle
342 of the 21st century (Fig. 7b). The greatest change occurs in winter. For summer, the
343 ensemble projects that the WVD almost remains unchanged during the middle of the
344 21st century while increases at the end of the 21st century. For autumn, the ensemble
345 projects that the WVD decreases slightly during the middle of the 21st century while
346 increases slightly by the end of the 21st century. The ensemble members show good
347 consistency of the projections for winter and annual mean during both periods.

348 4) Pearl River Delta economic zone

349 As projected by the ensemble (Fig. 8a), the annual, spring and summer AEC
350 would decrease. Such a decrease is relatively larger during the middle of the 21st
351 century than during the end of the 21st century and the greatest decrease occurs in
352 spring. For winter, the AEC is projected to increase and be comparable during the
353 middle and the end of the 21st century. For autumn, the projected AEC decreases by
354 about 1% over the period 2046-2065 and increase by about 0.5% over the period
355 2080-2099. However, the projections from the three members are not consistent for
356 all four seasons.

357 The ensemble projects an increase in WVD for annual mean and four seasons,
358 with the greatest increase in summer during the middle of the 21st century (Fig. 8b).
359 The individual members consistently show the positive change for spring, summer,
360 and annual mean. Compared with the middle of the 21st century, the increase of the
361 WVD is reduced in summer while enhanced for annual mean and the remaining
362 seasons during the late of the 21st century. The autumn is the season with the
363 maximum change. The individual members show the same projections as the
364 ensemble on the sign of change still for spring, summer, and annual mean.

365 The consistence of the three ensemble members on the direction of the projected
366 change which can be used to visualize the uncertainty in the projection is further
367 summarized in Table 3. In general, although there are some uncertainties on the
368 regional changes, the three members consistently project a decrease of the AEC or an
369 increase of WVD for annual mean over the four economic zones, especially over the

370 Beijing-Tianjin-Hebei region and Northeast China. It signifies that future climate
371 change will contribute positively to the haze pollution in these regions. For seasonal
372 change, decrease in AEC or increase in WVD, is projected consistently to appear in
373 all four seasons over Northeast China. It suggests that there would be an increase of
374 haze pollution potential throughout the whole year. Besides, the consistent projections
375 indicate a higher potential risk of haze pollution over the Beijing-Tianjin-Hebei
376 region and the Yangtze River Delta region in winter and over the Pearl River Delta
377 zone in spring and summer.

378 The temporal evolution of the annual and seasonal AEC and WVD over the four
379 main economic zones are also plotted (Figs. 5-8 c-g), and the corresponding trend
380 values projected by the ensemble for the period of 2016-2099 are summarized in
381 Table 4. Theil-Sen trend analysis (Theil, 1950; Sen, 1968) was used to estimate the
382 trends and the non-parametric Mann-Kendall test (Mann, 1945; Kendall, 1975) was
383 used for significant test. Generally, the secular variations of the AEC and the WVD
384 show some diversity across different seasons over the regions except NEC where a
385 decrease in AEC and an increase in WVD is projected uniformly. Nevertheless, for
386 the trends significant above the 95% level, it is interesting to notice that the decrease
387 in AEC is mostly accompanied with the increase in WVD, for instance for winter over
388 TBH, for annual mean and all the seasons over NEC, for annual mean, winter and
389 summer over YRD, and for annual mean and autumn over PRD.

390

391 **5 Contributions of different factors to the change of AEC**

392 Based on Eqs. (2) and (3), we further investigate the contribution of different
393 factors to the projected change in AEC. For brevity, we only show the results for the
394 period 2046-2065 in the following, because the case for the period 2080-2099 is
395 similar.

396 Figs. 9a and 9b exhibit relative contributions to the annual AEC change over the
397 course of 2046-2065 from changes in precipitation and ventilation, respectively.
398 Overall, the ventilation change plays a dominant role in and contributes positively to
399 the change of the AEC over most parts of China, particularly in western and northern
400 China (Fig. 9b). In contrast, the relative contribution of the precipitation change is in
401 general negative over western and northern China while positive over southern China
402 (Fig. 9a).

403 According to Eq. (3), the effect of ventilation change can be decomposed into
404 four terms, i.e., wind speed change, boundary layer depth change, nonlinear term, and
405 transient term. Among these contributors for annual ventilation change, the effects of
406 boundary layer depth (Fig.9d) and wind speed (Fig.9c) are relatively large and the
407 former is greater than the latter over most parts of eastern China. The transient term
408 also exert effects for instance over some parts of western and southern China (Fig.9f),
409 while the effects of the nonlinear term are tiny across China (Fig. 9e).

410 Fig. 10 further presents relative contributions of aforementioned factors to
411 annual and seasonal AEC change over the four economic zones as projected by the
412 ensemble and its members. As shown in Figs. 10a and 10b, changes in wind speed

413 and boundary layer depth have the greatest contributions to the AEC change over the
414 THB and NEC regions for annual mean and all the seasons except summer. The
415 contribution from the precipitation is in general relatively small. Besides, the effects
416 of the transient term are larger than that of the precipitation, and the effects of the
417 nonlinear term can be negligible. These results indicate that changes in wind speed
418 and boundary layer depth are the leading contributors responsible for the AEC change
419 over the two regions. In contrast, over the YRD (Fig.10c) and PRD (Fig.10d) zones,
420 change in precipitation also plays an important role. The contribution from the
421 precipitation change is comparable to and even larger than that from changes in wind
422 speed and boundary layer depth for all the seasons except winter.

423

424 **6 Conclusion**

425 In this study, we conducted downscaling simulations by use of the RegCM4
426 driven by three CMIP5 models' results under the historical simulation and the RCP4.5
427 scenario. On this basis, we evaluated the fidelity of the RegCM4 simulations on the
428 AEC and WVD which are indicators for haze pollution potential, and then projected
429 their change during the middle and the end of this century for China and four main
430 economic zones. The major findings are summarized below:

431 1) The evaluation indicates that the RegCM4 downscaling simulations in general
432 show good performance in modeling the climatological distribution of the annual and
433 seasonal AEC, despite some discrepancies in certain regions. The spatial correlations
434 between the simulation and the observation for annual mean and four seasons are

435 higher above 0.6. The simulations also well capture the observed WVD pattern with
436 relatively small WVD over Tibet and relatively large WVD over central and eastern
437 China, Northeast China, southern North China and Xinjiang, although the WVD is
438 overestimated systematically.

439 2) The annual AEC and WVD are respectively projected by the ensemble to
440 decrease and increase almost in the entire region except central China, accompanied
441 with larger amplitude by the end of the 21st century than by the middle of the 21st
442 century. The decreases in AEC are relatively large over Tibet, Southwest China,
443 northern North China, Northeast China and Inner Mongolia. The increase in WVD is
444 particularly pronounced in northern China. The individual members present consistent
445 projections of changes as the ensemble. In contrast, the ensemble projects an increase
446 in AEC and a decrease in WVD over central China. However, the sign of the
447 projected change is inconsistent among the ensemble samples.

448 3) The consistency analysis suggests that there would be a high probability of the
449 increase in air pollution risk over the BTH and YRD regions in winter and over the
450 PRD zone in spring and summer in a warmer world. Over NEC, climate change might
451 reduce the AEC or increase the WVD throughout the whole year, favorable for the
452 occurrence of haze pollution and also indicative of an aggravation of haze pollution
453 risk. Furthermore, the contribution analysis indicates that changes in boundary layer
454 depth and wind speed play the leading roles in the AEC change over the BTH and
455 NEC regions. In addition to the aforementioned two factors, the precipitation change
456 is also an important factor influencing the ACE change over the YRD and PRD zones.

457 In this study, we mainly showed the downscaled results driven by three global
458 models. Note that the planetary boundary layer depth is not a standard CMIP5 output
459 variable, and the coarse vertical resolution of the global models prevents us from
460 estimating the planetary boundary layer depth. These make it hard to estimate whether
461 the consistencies and inconsistencies of the projection is caused by the global models
462 or to some extent affected by the dynamical downscaling of the regional model.
463 Besides, it should be emphasized again that our study focused on the atmospheric
464 carrying capacity which is associated with the wet deposition and the ventilation. It is
465 just one of the contributors for the haze change. Other factors such as emission, wind
466 direction, relative humidity are also vital for the incident of haze. And the interaction
467 between aerosol and climate is another important issue (Qian et al., 2015; Li et al.,
468 2016). To get a full picture for future change of the haze, their effects need to be
469 studied by models with chemistry/aerosol module coupled in the future work.

470 **Acknowledgments.** This research was jointly supported by the National Key
471 Research and Development Program of China (2016YFA0600701), the National
472 Natural Science Foundation of China (41675069, 41405101), and the Climate Change
473 Specific Fund of China (CCSF201626, CCSF201731).

474 **References**

475 [Cai, W., Li, K., Liao, H., Wang, H., and Wu, L.: Weather conditions conducive to](#)
476 [Beijing severe haze more frequent under climate change, Nature Climate Change,](#)
477 [7, 257-262, 2017.](#)

478 Chen, H. P. and Wang, H. J.: Haze days in North China and the associated
479 atmospheric circulations based on daily visibility data from 1960 to 2012, J.
480 Geophys. Res. Atmos., 120, 5895–5909, doi:10.1002/2015JD023225, 2015.

481 Ding, Y. H., and Liu, Y. J.: Analysis of long-term variations of fog and haze in China
482 in recent 50 years and their relations with atmospheric humidity, Sci. China
483 Earth Sci., 57, 36–46, 2014.

484 Emanuel, K. A.: A scheme for representing cumulus convection in large-scale models,
485 J. Atmos. Sci., 48, 2313–2329, 1991.

486 Gao, G.: The climatic characteristics and change of haze days over China during
487 1961–2005, Acta Geogr. Sin., 63, 762–768, 2008.

488 Gao, X., Shi, Y., Zhang, D., Wu, J., Giorgi, F., Ji, Z., and Wang, Y.: Uncertainties in
489 monsoon precipitation projections over China: results from two high-resolution
490 RCM simulations, Clim. Res., 52, 213–226, 2012.

491 Gao, X., Shi, Y., and Giorgi, F.: Comparison of convective parameterizations in
492 RegCM4 experiments over China with CLM as the land surface model, Atmos.
493 Ocean. Sci. Lett., 9, 246–254, 2016a.

494 [Gao, X., Shi, Y., Han, Z., Wang, M., Wu, J., Zhang, D., Xu, Y., and Giorgi, F.:](#)
495 [Performance of RegCM4 over major river basins in China, Adv. Atmos. Sci., 34,](#)
496 [441-455, doi:10.1007/s00376-016-6179-7, 2017.](#)

497 ~~Gao, X., Shi, Y., Han, Z., Wang, M., Wu, J., Zhang, D., Xu, Y., and Giorgi, F.:~~
498 ~~Performance of RegCM4 over major river basins in China, Adv. Atmos. Sci.,~~
499 ~~doi:10.1007/s00376-016-6179-7, 2016b.~~

500 Giorgi, F., Jones, C., and Asrar, G.: Addressing climate information needs at the
501 regional level: the CORDEX framework, WMO Bull., 58, 175–183, 2009.

502 Giorgi, F., Coppola, E., Solmon, F., Mariotti, L., Sylla, M., Bi, X., Elguindi, N., Diro,
503 G., Nair, V., Giuliani, G., Turuncoglu, U., Cozzini, S., Güttler, I., O’Brien, T.,
504 Tawfik, A., Shalaby, A., Zakey, A., Steiner, A., Stordal, F., Sloan, L., and
505 Brankovic, C.: RegCM4: model description and preliminary tests over multiple
506 CORDEX domains, Clim. Res., 52, 7–29, 2012.

507 Goyal, S., and Rao, C. C.: Air assimilative capacity-based environment friendly siting
508 of new industries - A case study of Kochi region, India, J. Environ. Manage., 84,
509 473-483, 2007.

510 Guo, H., Xu, M., and Hu, Q.: Changes in near-surface wind speed in China: 1969–
511 2005, Int. J. Climatol., 31, 349–358, 2011.

512 Han, Z., Gao, X., Shi, Y., Wu, J., Wang, M., and Giorgi, F.: Development of Chinese
513 high resolution land cover for the RegCM4/CLM and its impact on regional
514 climate simulation (in Chinese), Journal of Glaciology and Geocryology, 37,
515 857–866, 2015.

516 He, H., Wang, X. M., Wang, Y. S., Wang, Z. F., Liu, J. G., Chen, Y. F., 2013:
517 Formation mechanism and control strategies of haze in China (in Chinese), Bull.
518 Chinese Acad. Sci., 28(3), 344–352.

519 Holtslag, A. A. M., De Bruijn, E. I. F., and Pan, H. L.: A high resolution air mass
520 transformation model for short-range weather forecasting, Mon. Wea. Rev., 118,
521 1561–1575, 1990.

522 IPCC: Climate Change 2013: The Physical Science Basis. Contribution of Working
523 Group I to the Fifth Assessment Report of the Intergovernmental Panel on Climate
524 Change, Cambridge University Press, Cambridge, United Kingdom and New
525 York, NY, USA, 1535pp, 2013.

526 ~~Kassomenos, P., Kotroni, V., and Kallos, G.: Analysis of climatological and air~~
527 ~~quality observations from greater Athens area, Atmos. Environ., 29, 3671–3688,~~
528 ~~1995.~~

529 ~~Manju, N., Balakrishnan, R., and Mani, N.: Assimilative capacity and pollutant~~
530 ~~dispersion studies for the industrial zone of Manali, Atmos. Environ., 36,~~
531 ~~3461–3471, 2002.~~

532 Jacob, D. J., and Winner, D. A.: Effect of climate change on air quality, Atmos.
533 Environ., 43, 51–63, 2009.

534 Jiang, Y., Luo, Y., and Zhao, Z. C.: Maximum wind speed changes over China, Acta
535 Meteorol. Sin., 27, 63–74, 2013.

536 Kang, Z., Gui, H., Hua, C., Zhang, B., Zhang, H., Lv, M., and Wang, J.: National
537 Environmental Meteorological Services in China, *Adv. Meteorol.*, 2016,
538 doi:10.1155/2016/1985207, 2016.

539 [Kassomenos, P., Kotroni, V., and Kallos, G.: Analysis of climatological and air](#)
540 [quality observations from greater Athens area, *Atmos. Environ.*, 29, 3671-3688,](#)
541 [1995.](#)

542 Kendall, M. G.: Rank Correlation Methods. Griffin, London, 1975.

543 Kiehl, J., Hack, J., Bonan, G., Boville, B., Williamson, D., and Rasch, P.: The
544 National Center for Atmospheric Research Community Climate Model: CCM3, *J.*
545 *Clim.*, 11, 1131–1149, 1998.

546 Krishnan, P., and Kunhikrishnan, P.: Temporal variations of ventilation coefficient at
547 a tropical Indian station using UHF wind profiler, *Curr. Sci.*, 86, 447–451, 2004.

548 Lee, J., and Hong, S.: Potential for added value to downscaled climate extremes over
549 Korea by increased resolution of a regional climate model, *Theor. Appl.*
550 *Climatol.*, 117, 667–677, 2014.

551 Leung, L. R., and Gustafson, W. I.: Potential regional climate change and
552 implications to US air quality, *Geophys. Res. Lett.*, 32, L16711, 2005.

553 Li, Q., Zhang, R. H., and Wang, Y.: Interannual variation of the winter-time fog–haze
554 days across central and eastern China and its relation with East Asian winter
555 monsoon, *Int. J. Climatol.*, 36, 346–354, doi:10.1002/joc.4350, 2015.

556 [Li, Z., Lau, W. K. M., Ramanathan, V., Wu, G., Ding, Y., Manoj, M. G., Liu, J., Qian,](#)
557 [Y., Li, J., Zhou, T., Fan, J., Rosenfeld, D., Ming, Y., Wang, Y., Huang, J., Wang,](#)

558 [B., Xu, X., Lee, S. S., Cribb, M., Zhang, F., Yang, X., Zhao, C., Takemura, T.,](#)
559 [Wang, K., Xia, X., Yin, Y., Zhang, H., Guo, J., Zhai, P. M., Sugimoto, N., Babu,](#)
560 [S. S., and Brasseur, G. P.: Aerosol and monsoon climate interactions over Asia,](#)
561 [Rev. Geophys., 54, 866-929, doi:10.1002/2015RG000500, 2016.](#)

562 Liu, J., and Diamond, J.: China's environment in a globalizing world, *Nature*, 435,
563 1179–1186, 2005.

564 [Manju, N., Balakrishnan, R., and Mani, N.: Assimilative capacity and pollutant](#)
565 [dispersion studies for the industrial zone of Manali, *Atmos. Environ.*, 36,](#)
566 [3461-3471, 2002.](#)

567 Mann, H. B.: Nonparametric tests against trend, *Econometrica*, 13, 245-259, 1945.

568 Oleson, K., Niu, G. Y., Yang, Z. L., Lawrence, D., Thornton, P., Lawrence, P.,
569 Stöckli, R., Dickinson, R., Bonan, G., and Levis, S.: Improvements to the
570 Community Land Model and their impact on the hydrological cycle, *J. Geophys.*
571 *Res.*, 113, G01021, 2008.

572 Pal, J. S., Small, E. E., and Eltahir, E. A. B.: Simulation of regional-scale water and
573 energy budgets: Representation of subgrid cloud and precipitation processes
574 within RegCM, *J. Geophys. Res.*, 105, 29579–29594, 2000.

575 Park, T. W., Deng, Y., and Cai, M.: Feedback attribution of the El Niño–Southern
576 Oscillation–related atmospheric and surface temperature anomalies, *Journal of*
577 *Geophysical Research: Atmospheres*, 117, D23101, doi:10.1029/2012jd018468,
578 2012.

579 Pimonsree, S.: PM10 dispersion during air pollution episode in Saraburi, Thailand,
580 Asia-Pacific Journal of Science and Technology, 13, 1185-1190, 2008.

581 [Qian, Y., Yasunari, T. J., Doherty, S. J., Flanner, M. G., Lau, W. K., Ming, J., Wang,](#)
582 [H., Wang, M., Warren, S. G., and Zhang, R.: Light-absorbing particles in snow](#)
583 [and ice: Measurement and modeling of climatic and hydrological impact, Adv.](#)
584 [Atmos. Sci., 32, 64-91, 2015.](#)

585 Sen, P. K.: Estimates of the regression coefficient based on Kendall's tau, Journal of
586 the American Statistical Association, 63, 1379-1389, 1968.

587 Song, L. C., Gao, R., Li, Y., and Wang, G. F.: Analysis of China's haze days in the
588 winter half-year and the climatic background during 1961–2012, Adv. Clim.
589 Change Res., 5, 1–6, 2014.

590 Taylor, K. E., Stouffer, B. J., and Meehl, G. A.: An overview of CMIP5 and the
591 experiment design, Bull. Am. Meteorol. Soc., 93, 485–498, 2012.

592 Theil, H.: A rank-invariant method of linear and polynomial regression analysis,
593 Proceedings of the Royal Netherlands Academy of Sciences, 53, I: 386–392, II:
594 521–525, III: 1397–1412, 1950.

595 Tian, D., Guo, Y., and Dong, W. J.: Future changes and uncertainties in temperature
596 and precipitation over China based on CMIP5 models. Adv. Atmos. Sci., 32,
597 487–496, doi:10.1007/s00376-014-4102-7, 2015.

598 Trail, M., Tsimpidi, A., Liu, P., Tsigaridis, K., Hu, Y., Nenes, A., and Russell, A.:
599 Downscaling a global climate model to simulate climate change over the US and

600 the implication on regional and urban air quality, *Geoscientific Model*
601 *Development*, 6, 1429, 2013.

602 Uppala, S., Dee, D., Kobayashi, S., Berrisford, P., and Simmons, A.: Towards a climate
603 data assimilation system: Status update of ERA-Interim, *ECMWF newsletter*, 115,
604 12–18, 2008.

605 Wang, H. J. and Chen, H. P.: Understanding the recent trend of haze pollution in
606 eastern China: roles of climate change, *Atmos. Chem. Phys.*, 16, 4205–4211,
607 doi:10.5194/acp-16-4205-2016, 2016.

608 Wang, H. J., Chen, H. P., and Liu, J. P.: Arctic sea ice decline intensified haze
609 pollution in eastern China, *Atmos. Ocean. Sci. Lett.*, 8, 1–9, 2015.

610 Wang, H. J., He, S. P., and Liu, J. P.: Present and future relationship between the East
611 Asian winter monsoon and ENSO: Results of CMIP5, *J. Geophys. Res. Ocean*,
612 118, 1–16, doi:10.1002/jgrc.20332, 2013a.

613 Wang, X. P. and Mauzerall, D. L.: Evaluating impacts of air pollution in China on
614 public health: implications for future air pollution and energy policies, *Atmos.*
615 *Environ.*, 40, 1706–1721, 2006.

616 Wang, Y. S., Yao, L., Liu, Z. R., Ji, D. S., Wang, L. L., and Zhang, J. K.: Formation of
617 haze pollution in Beijing-Tianjin-Hebei region and their control strategies, *Bull.*
618 *Chinese Acad. Sci.*, 28, 353–363, 2013b.

619 Wang, Z. F., Li, J., Wang, Z., Yang, W. Y., Tang, X., Ge, B. Z., Yan, P. Z., Zhu, L. L.,
620 Chen, X. S., Chen, H. S., Wang, W., Li, J. J., Liu, B., Wang, X. Y., Wang, W.,
621 Zhao, Y. L., Lu, N., and Su, D. W.: Modeling study of regional severe hazes

622 over Mid-Eastern China in January 2013 and its implications on pollution
623 prevention and control, *Sci. China: Earth Sci.*, 57, 3–13,
624 doi:10.1007/s11430-013-4793-0, 2014.

625 Wu, D., Tie, X., Li, C. C., Ying, Z. M., Lau, A. K., Huang, J., Deng, X. J., and Bi, X.
626 Y.: An extremely low visibility event over the Guangzhou region: A case study,
627 *Atmos. Environ.*, 39, 6568–6577, 2005.

628 Wu, D., Liao, G. L., Deng, X. J., Bi, X. Y., Tan, H. B., Li, F., Jiang, C. L., Xia, D.,
629 and Fan, S. J.: Transport condition of surface layer under haze weather over the
630 Pearl River Delta, *J. Appl. Meteorol. Sci.*, 19, 1–9, 2008.

631 Wu, J., Gao, X., Xu, Y., and Pan, J.: Regional climate change and uncertainty analysis
632 based on four regional climate model simulations over China, *Atmospheric and*
633 *Oceanic Science Letters*, 8, 147-152, 2015a.

634 Wu, J., Zhou, B. T., and Xu, Y.: Response of precipitation and its extremes over
635 China to warming: CMIP5 simulation and projection, *Chinese J. Geophys.*, 58,
636 3048-3060, doi: 10.6038/cjg20150903, 2015b.

637 Xu, D., and Zhu, R.: A study on the distribution of ventilation and rainout capacity in
638 mainland China (in Chinese), *China Environ. Sci.*, 9, 367-374, 1989.

639 Xu, P., Chen, Y. F., and Ye, X. J.: Haze, air pollution, and health in China, *Lancet*,
640 382, 2067, doi:10.1016/S0140-6736(13)62693-8, 2013.

641 Xu, Y., and Xu, C. H., Preliminary assessment of simulations of climate changes over
642 China by CMIP5 multi-models, *Atmos. Ocean. Sci. Lett.*, 5, 489–494, 2012.

643 [Yang, Y., Liao, H., and Lou, S.: Increase in winter haze over eastern China in recent](#)

644 [decades: Roles of variations in meteorological parameters and anthropogenic](#)

645 [emissions, Journal of Geophysical Research: Atmospheres, 121, 2016.](#)

646 Yin, Z. C., Wang, H. J., and Guo, W. L.: Climatic change features of fog and haze in

647 winter over North China and Huang-Huai Area, *Sci. China Earth Sci.*, 58, 1370–

648 1376, 2015.

649 Zhang, R. H., Li, Q., and Zhang, R. N.: Meteorological conditions for the persistent

650 severe fog and haze event over eastern China in January 2013, *Sci. China: Earth*

651 *Sci.*, 57, 26–35, 2014.

652 [Zou, Y., Wang, Y., Zhang, Y., and Koo, J.-H.: Arctic sea ice, Eurasia snow, and](#)

653 [extreme winter haze in China, Science Advances, 3, e1602751, 2017.](#)

654

655 **Captions:**

656 **Table 1.** Statistic results for the simulation skills in annual mean AEC for the period
657 of 1986-2005.

658 **Table 2.** Statistic results for the ensemble simulation skills in seasonal AEC for the
659 period of 1986-2005.

660 **Table 3.** The consistence of the three ensemble members on the direction of the
661 projected change over the four economic zones of China. Consistent projection
662 on the decrease in AEC is marked by \surd and that on the increase in WVD is
663 marked by \star .

664 **Table 4.** Trends of AEC and WVD (%/10a) over the four economic zones of China,
665 based on 9-year running mean time series of the percentage change during
666 2016-2099. Asterisks indicate the trends are statistically significant above the 95%
667 confidence level.

668 **Figure 1.** Spatial distribution of annual AEC (unit: 10^4t/a/km) during 1986-2005: (a)
669 observation, (b) ensemble, (c) EC, (d) HAD, (e) MPI. (f) Four main economic
670 zones of China, Beijing-Tianjin-Hebei region (BTH), Northeast China (NEC),
671 Yangtze River Delta economic zone (YRD), and Pearl River Delta economic
672 zone (PRD).

673 **Figure 2.** Spatial distribution of seasonal AEC (unit: 10^4t/a/km) during 1986-2005:
674 (a-b) winter, (c-d) spring, (e-f) summer, (g-h) autumn. Left panel is for the
675 observation and the right panel is for the ensemble simulation.

676 **Figure 3.** Spatial distribution of (a-b) the number of weak ventilation days per year
677 and (c-d) wet deposition (unit: 10^4t/a/km) during 1986-2005: (a, c) observation,
678 (b, d) ensemble simulation.

679 **Figure 4.** Ensemble projected percentage changes (relative to 1986-2005) in (a-b)
680 AEC and (c-d) WVD during (a, c) 2046-2065 and (b, d) 2080-2099. Hatched
681 regions indicate all ensemble members agree on the sign of change.

682 **Figure 5.** Range of projected percentage changes (relative to 1986-2005) in (a) AEC
683 and (b) WVD during 2046-2065 and 2080-2099, and 9a running mean time series
684 of percentage changes in (c) annual, (d) winter (DJF), (e) spring (MAM), (f)
685 summer (JJA), (g) autumn (SON) for the Beijing-Tianjin-Hebei region. In Figure
686 (a-b), the bars represent the ensemble projection and the marks represent the
687 individual projection of the three members; the left (right) bar in each group is for
688 2046-2065 (2080-2099). In Figure (c-g), the solid (dashed) lines represent
689 changes in AEC (WVD).

690 **Figure 6.** Same as Figure 5, but for Northeast China.

691 **Figure 7.** Same as Figure 5, but for Yangtze River Delta economic zone.

692 **Figure 8.** Same as Figure 5, but for Pearl River Delta economic zone.

693 **Figure 9.** Relative contributions (unit: %) of individual components to annual AEC
694 change in the middle of the 21st century based on the ensemble results. (a)
695 precipitation, (b) ventilation, (c) wind speed averaged with the boundary layer, (d)
696 boundary layer depth, (e) nonlinear term, (f) transient term.

697 **Figure 10.** Relative contributions (unit: %) of individual components to annual AEC
698 change in the middle of the 21st century averaged over four main economic
699 zones of China: (a) BTH, (b) NEC, (c) YRD, (d) PRD. The bars represent the
700 ensemble projection and the marks represent the individual projection of the three
701 members. Bars from left to right in each group are in turn for annual, DJF, MAM,
702 JJA, and SON.

703 **Table 1.** Statistic results for the simulation skills in annual mean AEC for the period
704 of 1986-2005.

Simulations	Pattern correlation coefficient (CC)	Root mean square error (RMES)
EC	0.76	0.47
HAD	0.79	0.53
MPI	0.76	0.47
Ensemble	0.77	0.48

705

706 **Table 2.** Statistic results for the ensemble simulation skills in seasonal AEC for the
707 period of 1986-2005.

Season	Pattern correlation coefficient (CC)	Root mean square error (RMES)
Winter	0.79	0.75
Spring	0.75	0.67
Summer	0.60	0.57
Autumn	0.78	0.47

708

709 **Table 3.** The consistence of the three ensemble members on the direction of the
 710 projected change over the four economic zones of China. Consistent projection on the
 711 decrease in AEC is marked by \checkmark and that on the increase in WVD is marked by
 712 \star .

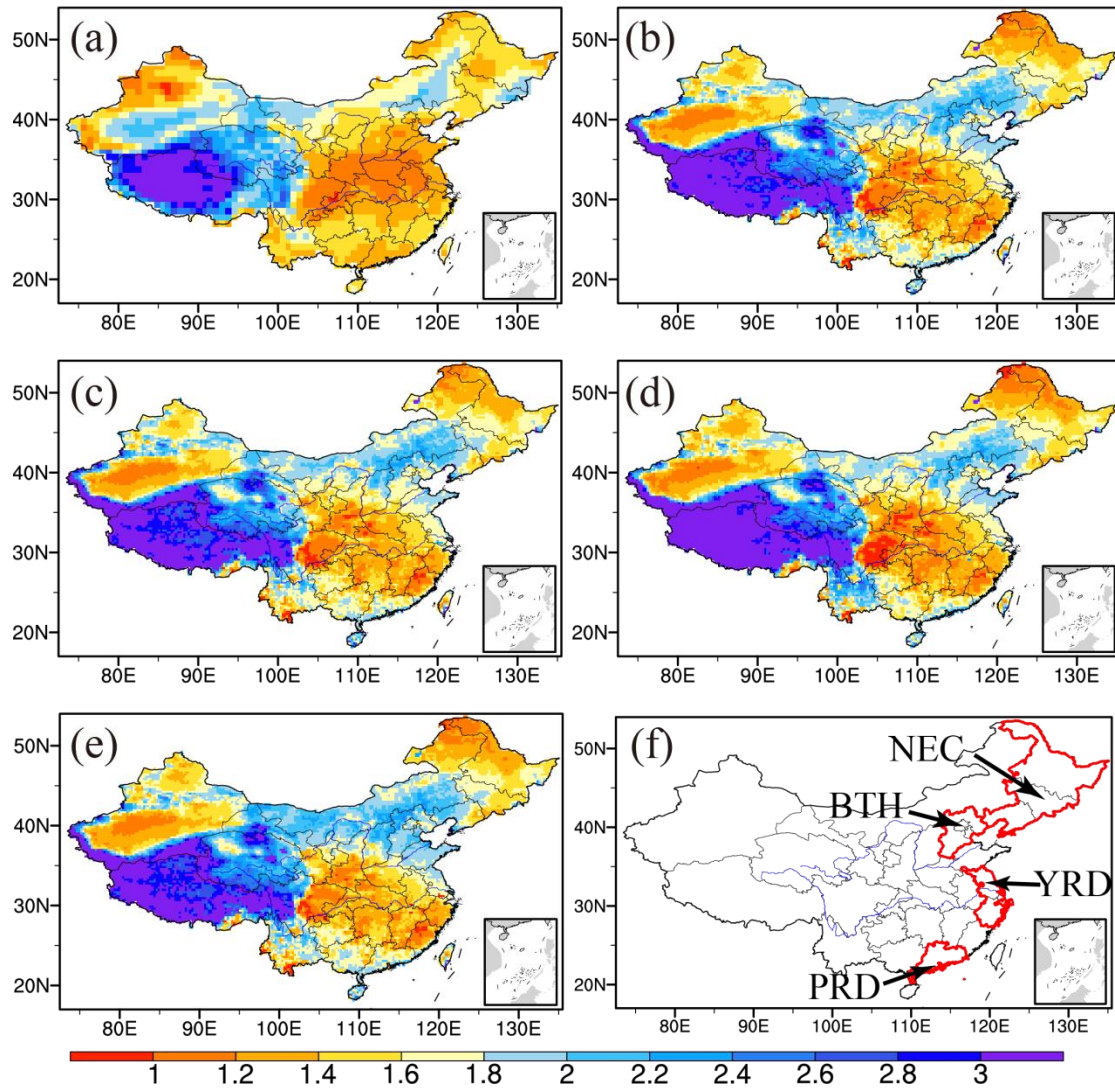
Economic zone	Period	ANN	DJF	MAM	JJA	SON
BTH	2046-2065	$\checkmark \star$	$\checkmark \star$		\checkmark	$\checkmark \star$
	2080-2099	$\checkmark \star$	\star			
NEC	2046-2065	$\checkmark \star$	$\checkmark \star$	\star	$\checkmark \star$	$\checkmark \star$
	2080-2099	$\checkmark \star$	$\checkmark \star$	$\checkmark \star$	$\checkmark \star$	$\checkmark \star$
YRD	2046-2065	$\checkmark \star$	$\checkmark \star$			
	2080-2099	\star	$\checkmark \star$			
PRD	2046-2065	\star		\star	\star	
	2080-2099	\star		\star	\star	

713

714 **Table 4.** Trends of AEC and WVD (%/10a) over the four economic zones of China,
715 based on 9-year running mean time series of the percentage change during 2016-2099.
716 Asterisks indicate the trends are statistically significant above the 95% confidence
717 level.

Economic zone	Variable	ANN	DJF	MAM	JJA	SON
BTH	AEC	-0.41*	-0.96*	0.02	-0.19*	-0.80*
	WVD	0.33	2.30*	-1.53*	-0.51*	0.55
NEC	AEC	-0.46*	-0.76*	-0.26*	-0.41*	-0.61*
	WVD	1.49*	2.60*	1.30*	0.73*	0.97*
YRD	AEC	-0.27*	-1.17*	0.32*	-0.45*	-0.02
	WVD	0.51*	0.88*	-0.26	0.71*	-0.15
PRD	AEC	-0.14*	-0.03	-0.22*	-0.12	-0.29*
	WVD	1.17*	-0.01	-0.30	2.17*	1.50*

718



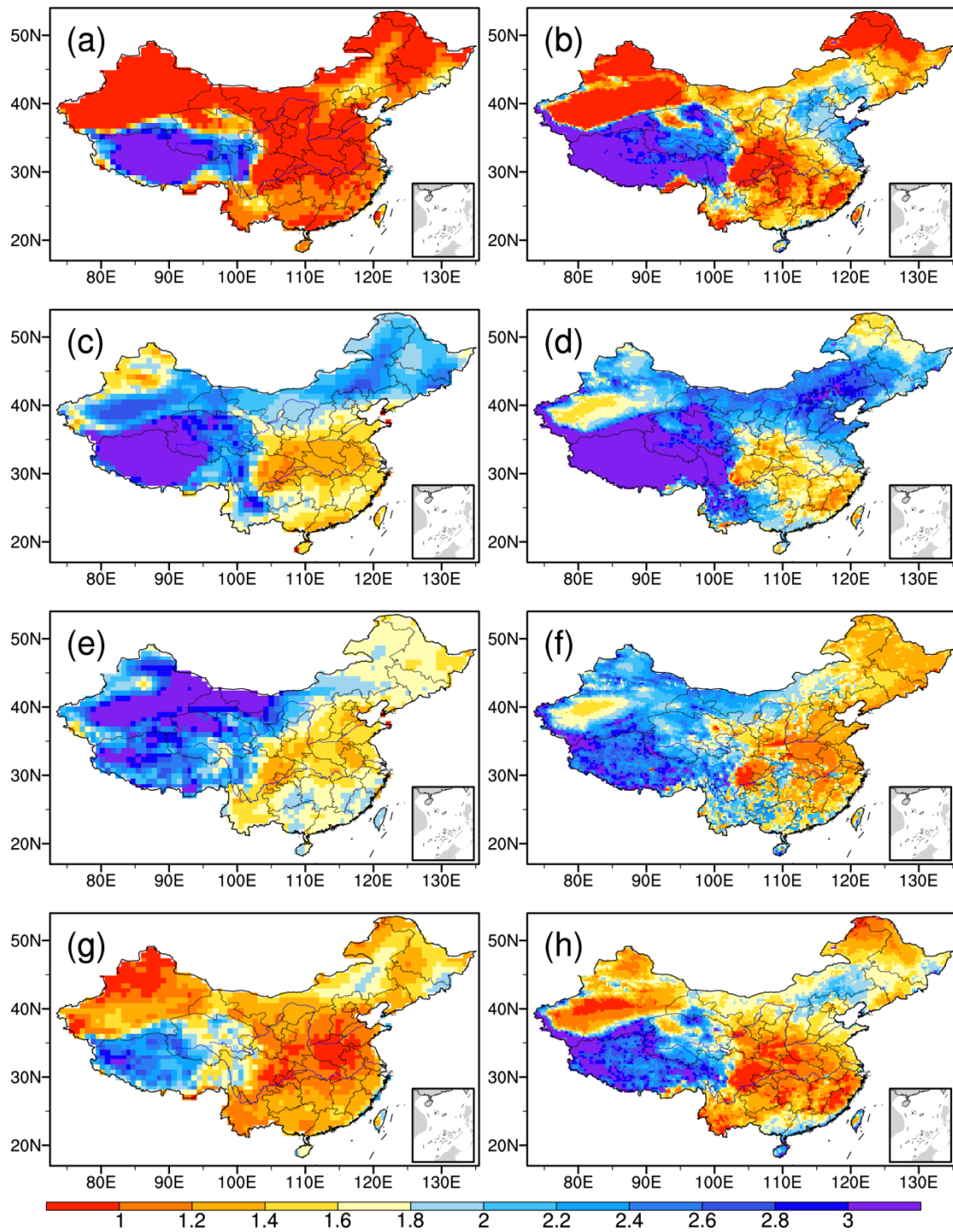
720

721 **Figure 1.** Spatial distribution of annual AEC (unit: 10^4 t/a/km) during 1986-2005: (a)

722 observation, (b) ensemble, (c) EC, (d) HAD, (e) MPI. (f) Four main economic zones

723 of China, Beijing-Tianjin-Hebei region (BTH), Northeast China (NEC), Yangtze

724 River Delta economic zone (YRD), and Pearl River Delta economic zone (PRD).

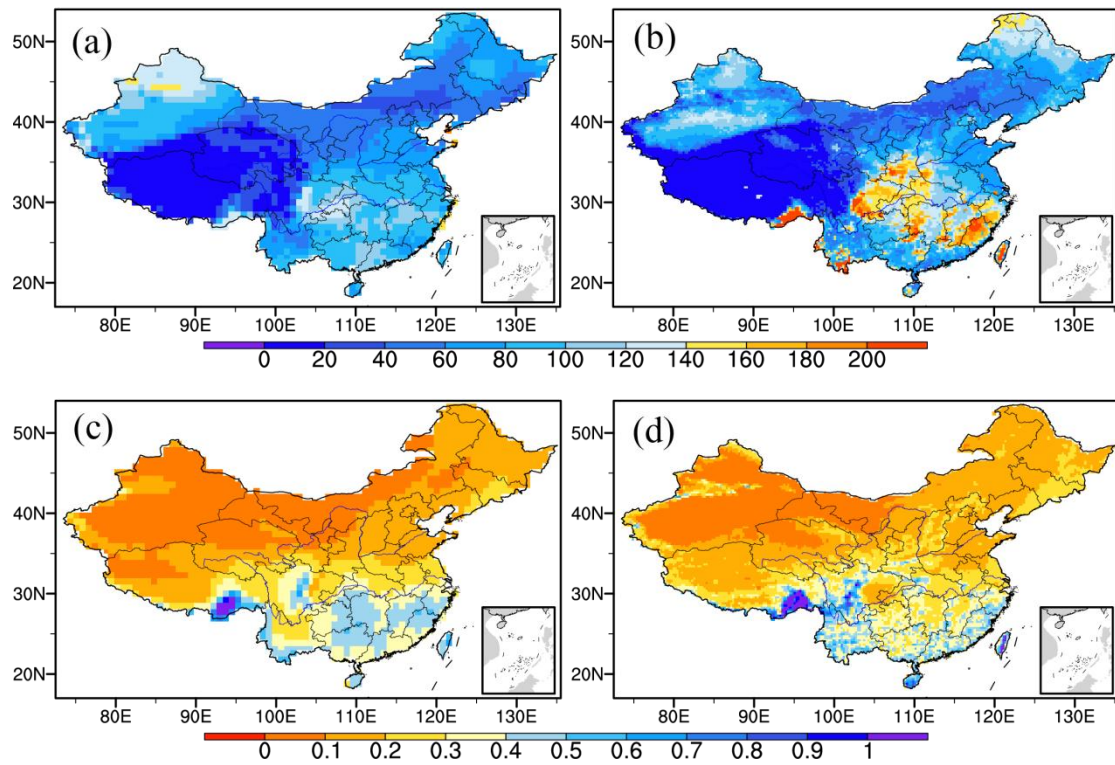


726

727 **Figure 2.** Spatial distribution of seasonal AEC (unit: 10^4 t/a/km) during 1986-2005:

728 (a-b) winter, (c-d) spring, (e-f) summer, (g-h) autumn. Left panel is for the

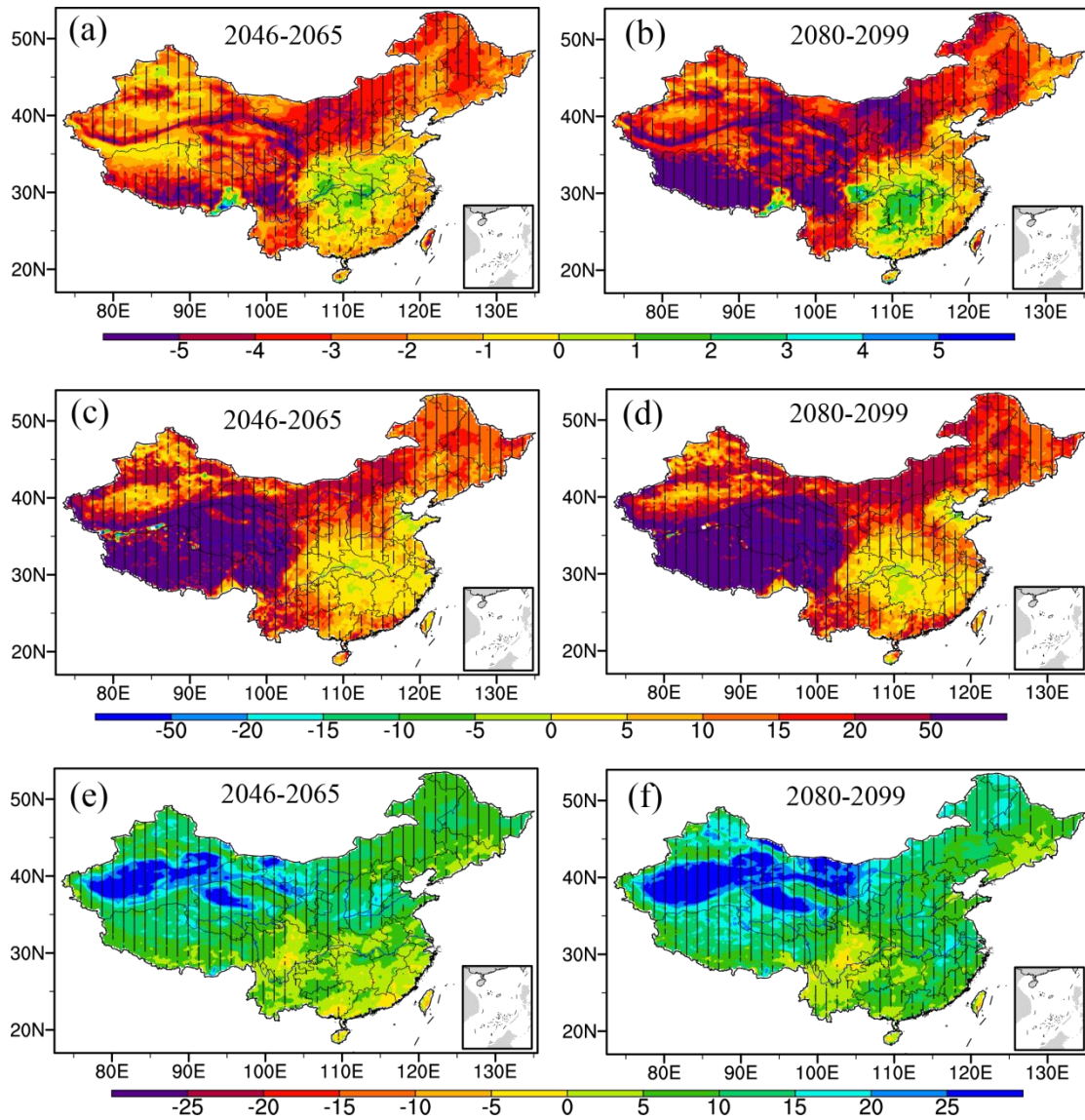
729 observation and the right panel is for the ensemble simulation.



731

732 **Figure 3.** Spatial distribution of (a-b) the number of weak ventilation days per year733 and (c-d) wet deposition (unit: 10^4 t/a/km) during 1986-2005: (a, c) observation, (b, d)

734 ensemble simulation.



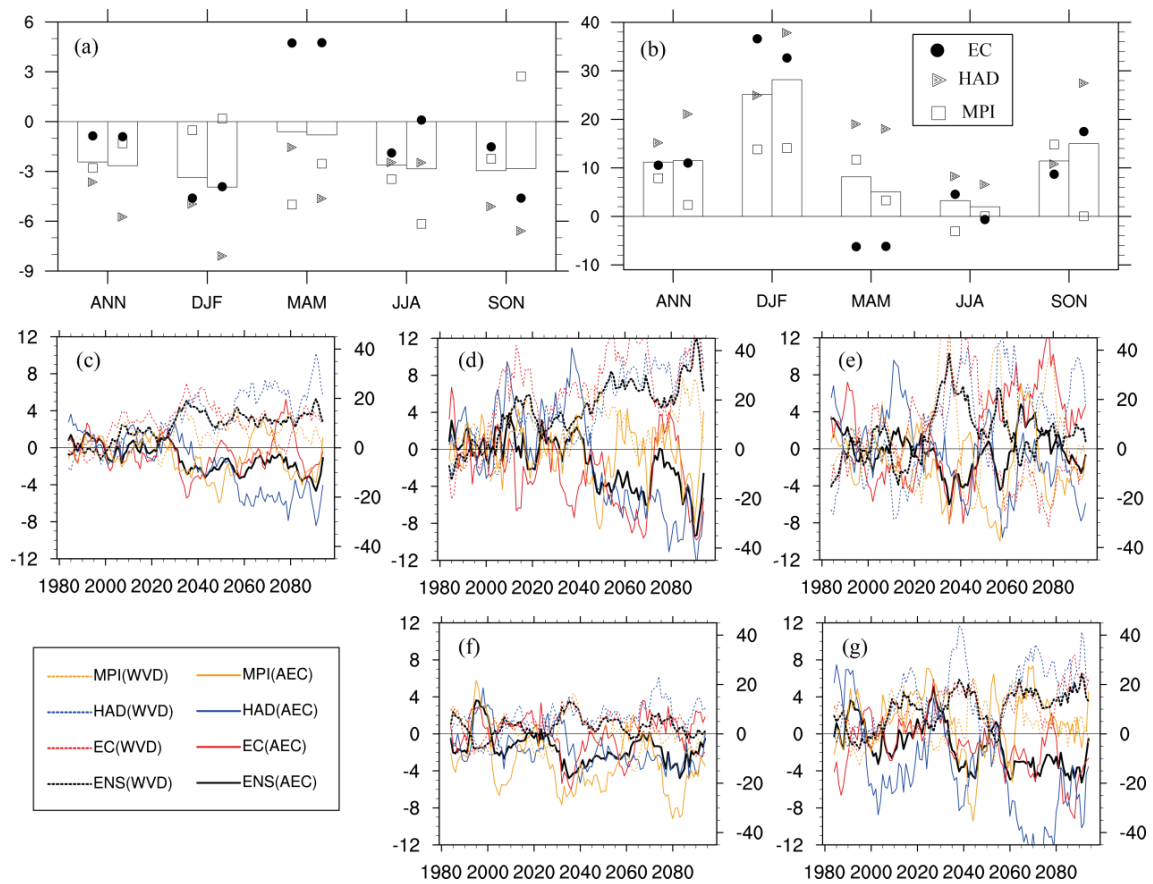
735

736 **Figure 4.** Ensemble projected percentage changes (relative to 1986-2005) in (a-b)

737 AEC, (c-d) WVD, and (e-f) wet deposition during 2046-2065 (left panel) and

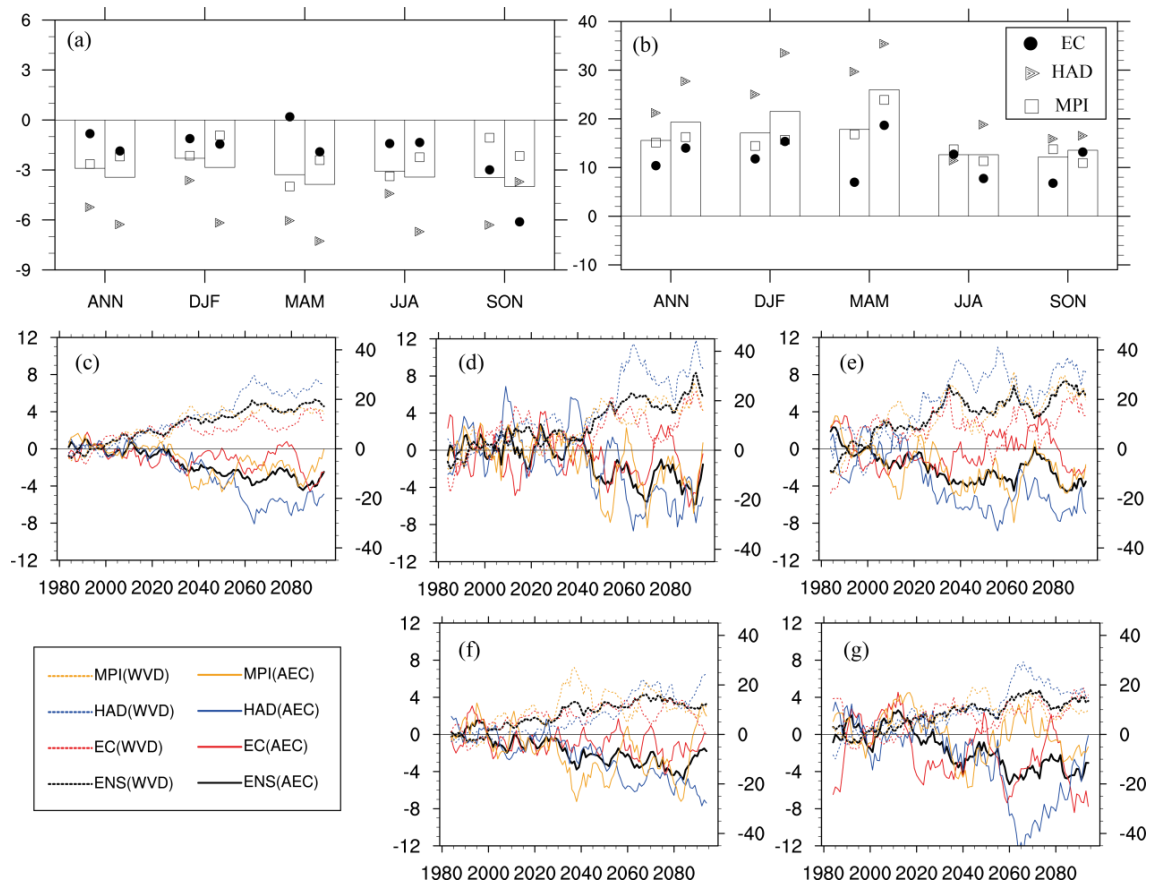
738 2080-2099 (right panel). Hatched regions indicate all ensemble members agree on the

739 sign of change.



740

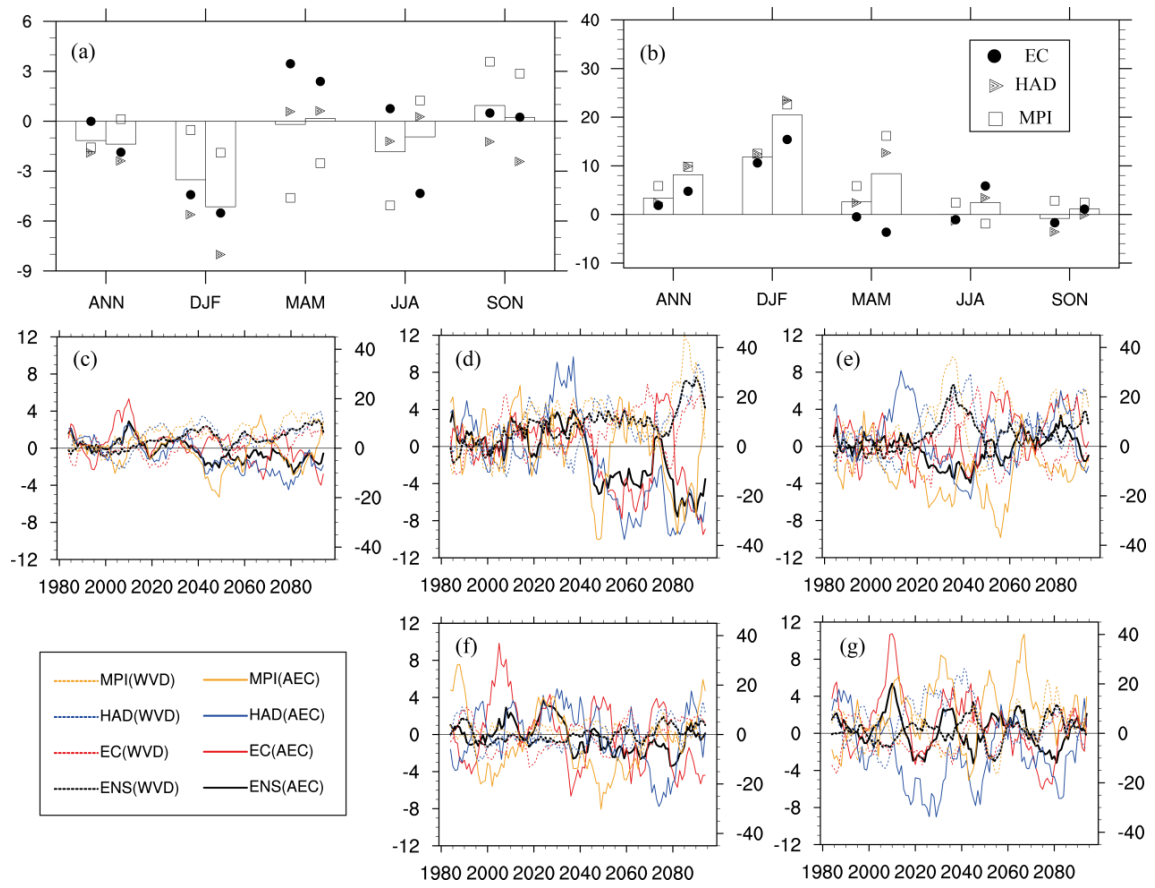
741 **Figure 5.** Range of projected percentage changes (relative to 1986-2005) in (a) AEC
 742 and (b) WVD during 2046-2065 and 2080-2099, and 9a running mean time series of
 743 percentage changes in (c) annual, (d) winter (DJF), (e) spring (MAM), (f) summer
 744 (JJA), (g) autumn (SON) for the Beijing-Tianjin-Hebei region. In Figure (a-b), the
 745 bars represent the ensemble projection and the marks represent the individual
 746 projection of the three members; the left (right) bar in each group is for 2046-2065
 747 (2080-2099). In Figure (c-g), the solid (dashed) lines represent changes in AEC
 748 (WVD).



749

750

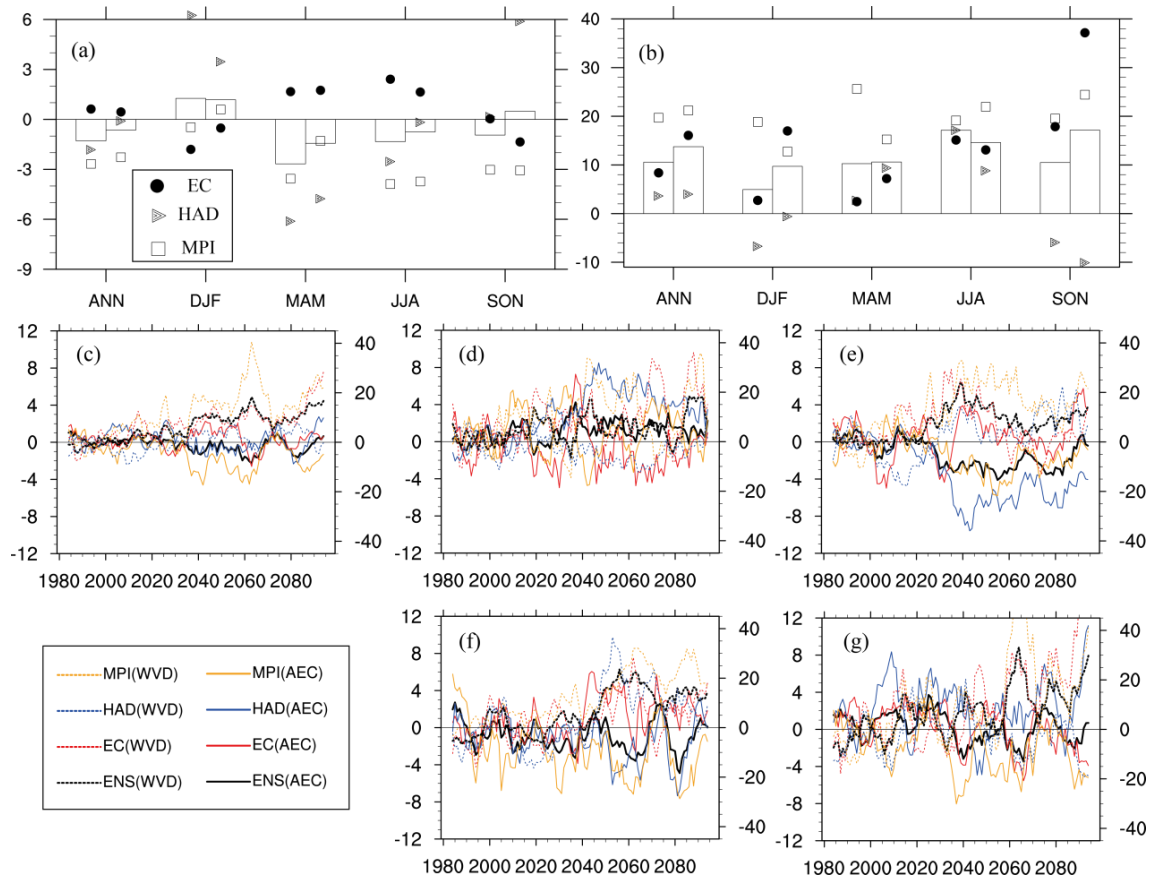
Figure 6. Same as Figure 5, but for Northeast China.



751

752

Figure 7. Same as Figure 5, but for Yangtze River Delta economic zone.

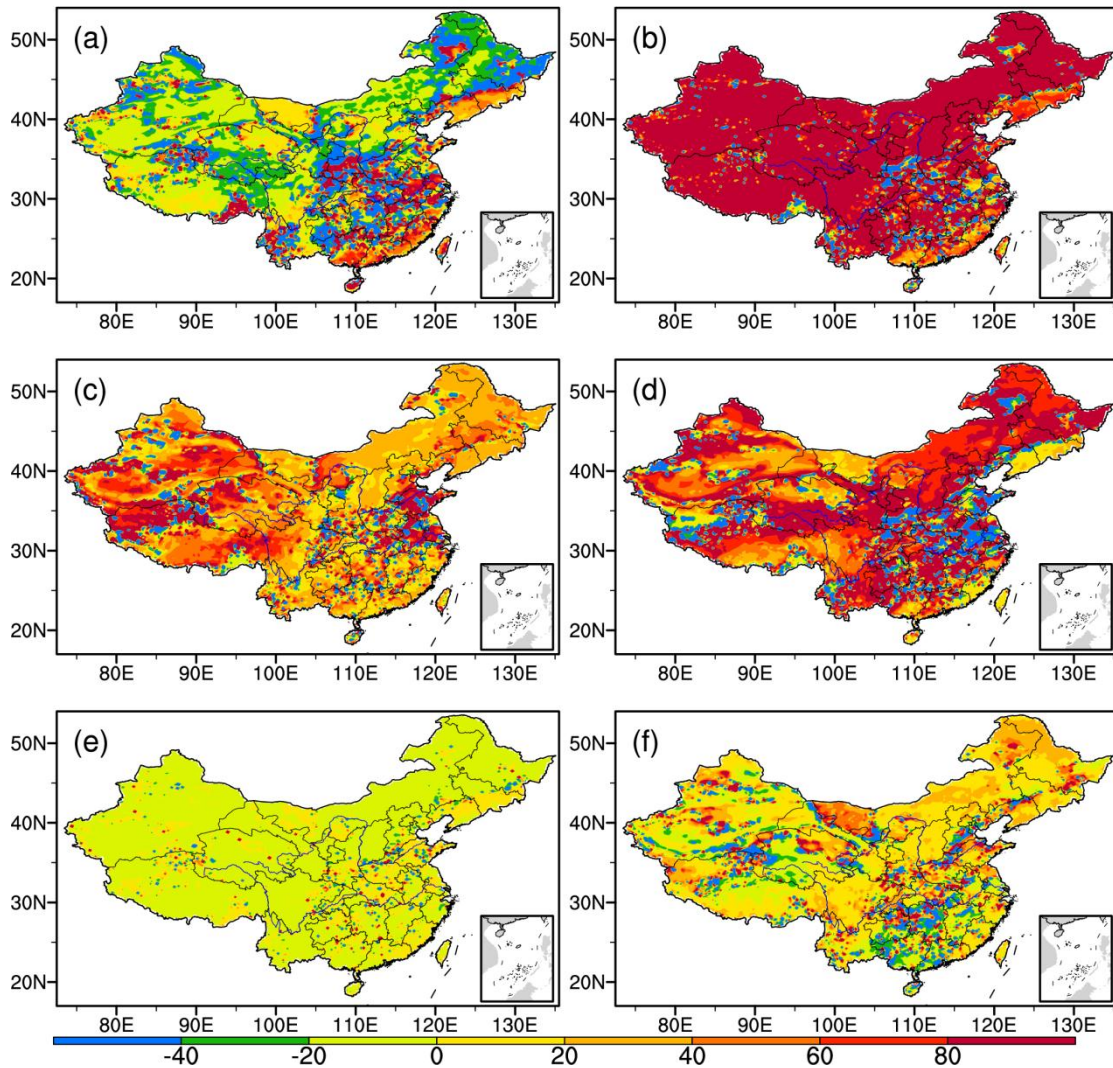


753

754

Figure 8. Same as Figure 5, but for Pearl River Delta economic zone.

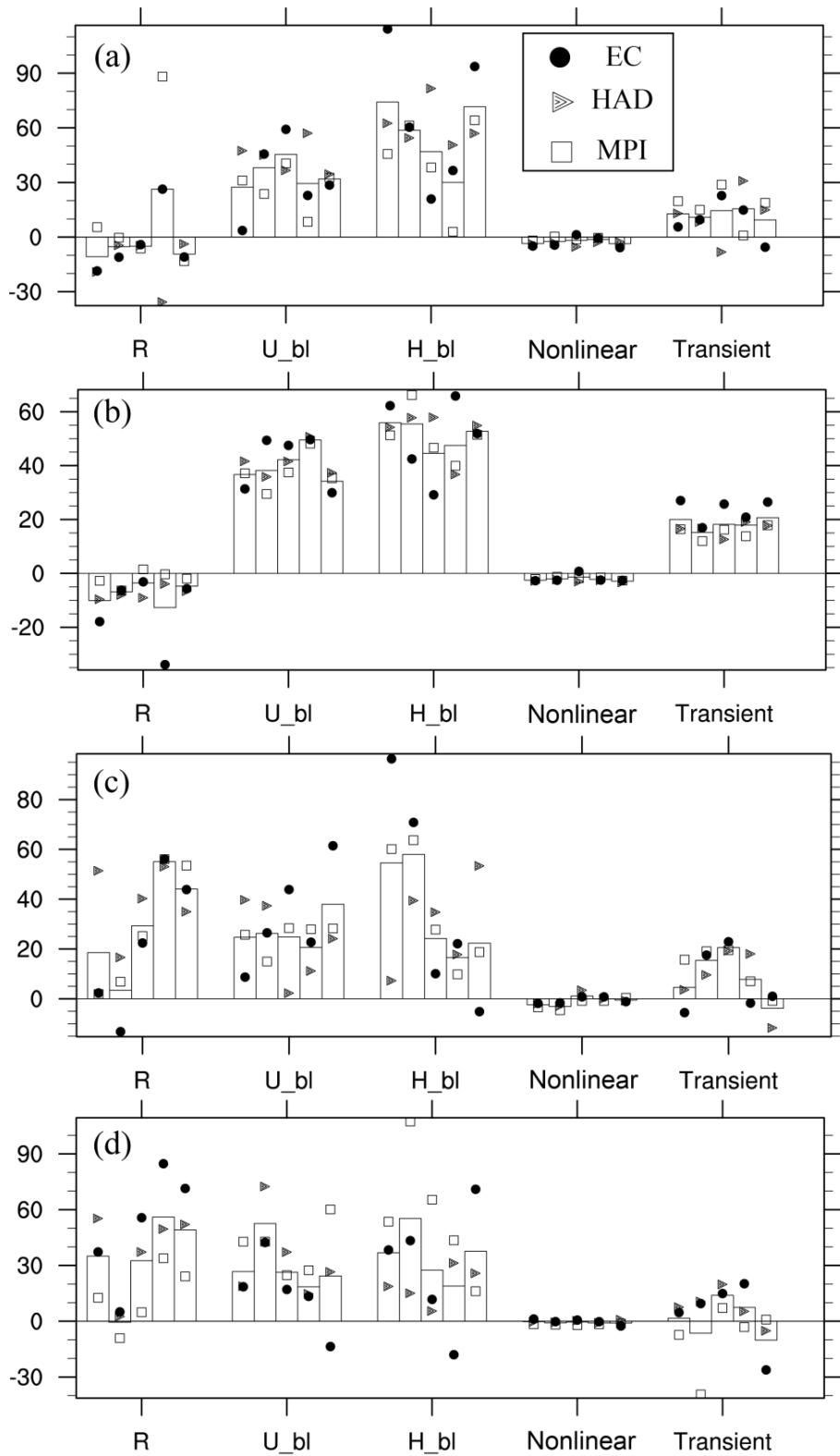
755



756

757 **Figure 9.** Relative contributions (unit: %) of individual components to annual AEC
 758 change in the middle of the 21st century based on the ensemble results. (a)
 759 precipitation, (b) ventilation, (c) wind speed averaged with the boundary layer, (d)
 760 boundary layer depth, (e) nonlinear term, (f) transient term.

761



762

763 **Figure 10.** Relative contributions (unit: %) of individual components to annual AEC

764 change in the middle of the 21st century averaged over four main economic zones of

765 China: (a) BTH, (b) NEC, (c) YRD, (d) PRD. The bars represent the ensemble

766 projection and the marks represent the individual projection of the three members.

767 Bars from left to right in each group are in turn for annual, DJF, MAM, JJA, and

768 SON.